Islamic Azad University

Journal of

Optoelectronical Nanostructures

Spring 2023 / Vol. 8, No. 2

Research Paper

Optical Properties of NiO Columnar Nanostructure Prepared by OAD Technique

Mohammad Hadi Karimi Tafti*[,1], Mahsa Fakharpour[2]

[1] Department of Electrical Engineering, Mehriz Branch, Islamic Azad University, Mehriz, Iran.
[2] Department of Physics, Maybod Branch, Islamic Azad University, Maybod, Iran.

Received: 16 Apr. 2023
Revised: 17 May. 2023
Accepted: 05 Jun. 2023
Published: 10 Jun. 2023

Use your device to scan and read the article online

Keywords:
Columnar nanostructure, Energy bandgap, NiO thin film, Optical constants.

Abstract:
NiO columnar nanostructure was prepared using the thermal evaporation technique with oblique angle deposition (OAD). The morphological, structural, and optical properties change with the creation of the substrate inclination. NiO columnar nanostructure was analyzed using X-ray diffraction (XRD) analysis and field emission scanning electron microscope (FESEM). The strain values ε obtained exhibit that the strain becomes tensile ($\varepsilon>0$) for (2 0 0) and (2 2 2) planes. Conversely, the strain returns to a compressive state ($\varepsilon<0$) for (1 1 1) and (2 2 0) planes. The average tensile strain in NiO columnar nanostructure is obtained at 1.4% while the average compressive strain is obtained at 2.04%. The value of the optical bandgap of the NiO columnar nanostructure is obtained at about 4.06 eV. The refractive index showed two absorption bands around the wavelengths of 520 nm and 700 nm with values of 2.19 and 2.22, respectively. Then, the refractive index increased from 2.22 at 700 nm to 2.35 at 920 nm and remained almost constant over 920 nm.

Citation: Mohammad Hadi Karimi Tafti, Mahsa Fakharpour. Optical properties of NiO columnar nanostructure prepared by OAD technique. **Journal of Optoelectronical Nanostructures. 2023; 8 (2): 51-67. DOI: 10.30495/JOPN.2023.31332.1277**

***Corresponding author:** Mohammad Hadi Karimi Tafti
Address: Department of Electrical Engineering, Mehriz Branch, Islamic Azad University, Mehriz, Iran. **Tell:** 00989131535583 **Email:** dr.karimitafti@gmail.com

1. INTRODUCTION

NiO is a subgroup of p-type semiconductors that have been of interest to many researchers due to its wide and direct optical bandgap of about 3.6 to 4.0 eV [1]. Due to its optical properties, high transparency in the visible region, electrical, magnetic, and chemical stability, it is a suitable choice for a widespread range of applications such as solar cells [2,3], chemical sensors [4], anti-ferromagnetic materials [5], UV detectors [6], smart windows [7] and so on. Many different techniques have been used to fabricate nickel oxide films such as physical vapor deposition (PVD) [8], sputtering [9,10], sol-gel deposition [11], pulsed laser deposition [12,13], electron beam evaporation [5,14], and so on. Among these methods, physical evaporation deposition is preferable to other methods due to the control of thickness and morphology of the structure and the possibility of making two- and three-dimensional nanostructures without the need to target. In this deposition, the incident vapor atoms reach the substrate obliquely and it is called the oblique angle deposition (OAD) method, which is a new technique for preparing different columnar nanostructures [15]. The main mechanism of this deposition is based on self-shadowing and growth competition. At first, the nuclei are formed on the substrate, then with the growth of the nuclei, the self-shadowing effect increases, and as a result, structures with different morphology such as columnar, chiral, square, zigzag are formed [16-18]. One of the characteristics of these nanostructures is their porosity, which can offer different optical properties. Sarkar et al. [19] provided multi-layer silicon coatings with anti-reflection properties by OAD and RF magnetron sputtering techniques. They showed that the porosity and the flux incidence angle affect the refractive index of the layers. The dependence of the deposition parameters on the microstructure and electrical properties of tungsten layers was investigated by Potin et al. [20]. The parameters such as pressure and current during deposition affect the electrical conductivity and morphology of nanocolumnar layers. The electrochemical properties of NiO nanorods fabricated using the sputtering technique were investigated by Tyagi et al. [21]. To use nickel oxide in supercapacitors, Kannan et al. [22] prepared NiO nanorods using the OAD technique and investigated the effect of nanorod dimensions on their electrical properties. In another study, columnar nanostructures on Si (100) substrate under different incident angles was studied by magnetron sputtering with oblique angle deposition technique and the results showed that the morphology of nanocolumns and their optical properties depend on the angle of incident flux [23]. Very little research is available on 3D NiO

nanostructures and studying their optical parameters.

Very little research is available on three-dimensional NiO nanostructures and the study of their optical parameters. In this research, we prepared NiO columnar structure on a glass substrate using OAD and thermal evaporation methods. Characteristics and morphology of the columnar structure were performed by X-ray diffraction (XRD) and field emission scanning electron microscopy (FESEM), respectively. The optical properties of these films were obtained using spectrophotometry. The aim of the present work is the synthesis, and study of energy bandgap and optical constants of NiO columnar nanostructure by the OAD method. The optical properties of deposited films were measured using spectrophotometry in the spectral range of 200-1100 nm. Therefore, the optical properties in the visible region and the wide bandgap expand the application of this columnar nanostructure to solar cells, optoelectronics, anti-reflective coatings, and so on.

Section 1 deals with the statement of the problem. In Section 2, the method of testing and preparation of nickel oxide columnar nanostructure is presented. Section 3 provides the results of various analyzes of the nanostructure, and Sec. 4 provides an interpretation of the results and suggestions for future directions of this work.

2. EXPERIMENTAL DETAILS

NiO powder with 99.99% purity from the Merck brand has been used to prepare columnar nickel oxide nanostructures on a glass substrate. The deposition was done at room temperature by the thermal evaporation method. A tungsten boat is used for the evaporation source. The glass substrates with dimensions of 2 cm ×2 cm was ultrasonically cleaned first in acetone for 15 min and then in ethanol for the same period. The substrates were glued on a stainless steel holder with a diameter of 10 cm. During deposition, the base pressure of the chamber was kept at 2×10^{-6} torr. The nickel oxide vapor flux fell on the substrates at an angle of 35º to the horizontal axis to form oblique columnar nanostructures. The deposition was performed at a rate of 0.3 nm/s. The thickness of NiO thin films with tilted columns was 490±20 nm. Using an X-ray diffraction device (Philips PW1730, Japan), the structural properties of columnar nanostructures were investigated in the 2θ range of 35º – 80º. The surface and cross-sectional images of the samples were analyzed using a field emission scanning electron microscope (FESEM, TESCAN, MIRA III) to analyze the morphology of the nanostructure and the thickness of the layers. The

transmittance and reflectance spectra were taken by a UV-Vis spectrophotometer (PerkinElmer - Lambda25) to study optical properties.

3. RESULTS AND DISCUSSION

A. Structural properties

1) X-ray diffraction

Fig. 1 displays the XRD pattern of the NiO columnar nanostructure on the glass substrate. The four diffraction peaks at 37.44º, 43.47º, 63.20º, and 79.87º were assigned to the (1 1 1), (2 0 0), (2 2 0), and (2 2 2) diffraction planes. These peaks were identified by JCPDS with the number 00-001-1239 and indicate a face-centered lattice with polycrystalline properties. The crystalline orientation of the film depends on the nuclei formed on the substrate and the growth of the grains [24]. Also, fluctuations in the spectrum indicate the effect of the substrate (glass) on the morphology of the nanostructure. The diffraction peaks formed in the XRD spectrum of NiO nano-columnars are consistent with the results of Kanan et al. [22], who prepared the NiO nanostructure by the same method. Horprathum et al. [23] also showed that the crystallinity of NiO films by the OAD method depends on the deposition angle and the formation of nanostructures during the growth process.

The average crystal grain size (D) of the NiO columnar nanostructure was estimated from Scherrer's equation [25]:

$$D = \frac{\kappa\lambda}{\beta\cos\theta}, \tag{1}$$

where λ=*1.5418* ◌̊A, k = *0.9*, θ, and β are the wavelength of Cu-Kα radiation, shape factor, Bragg diffraction angle, and FWHM, respectively. The data obtained from X-ray diffraction are given in Table 1. The average crystallite size of NiO columnar nanostructure was calculated at about 22.77 nm. Decreasing the FWHM leads to an increase in the grain size of the NiO columnar nanostructure.

Using the Bragg equation, the lattice constant (a) of the cubic structure can be calculated [25]:

$$2d\sin\theta = n\lambda, \tag{2}$$

$$\frac{1}{d^2} = \left(\frac{h^2+k^2+l^2}{a^2}\right), \tag{3}$$

where *(h k l)* are Miller indices and d is the inter-planer distance. The average lattice constant of the NiO columnar nanostructure was obtained at about 0.4142

nm which was different from 0.4155 nm of the standard value (JCPDS 00-001-1239).

Strain (ε) indicates the displacement of the atom from the location of its main lattice [26]. Therefore, the strain value ε is related to the lattice constant a as follows:

$$\varepsilon = \frac{a - a_0}{a_0} \times 100\%, \quad (4)$$

where a_0 and a are the bulk material and the measured lattice constant, respectively.

Along the (2 0 0) and (2 2 2) directions, the lattice constant a is greater than a_0, thus the unit cell is stretched in these directions, creating a tensile force. The strain values ε obtained exhibit that the strain becomes tensile ($\varepsilon>0$) for (2 0 0) and (2 2 2) planes. Conversely, the strain returns to a compressive state ($\varepsilon<0$) for (1 1 1) and (2 2 0) planes.

Dislocation density (δ) is a defect in the crystal that is associated with lattice mismatch between different parts of the crystal [23]. The value δ is calculated as follows [27]:

$$\delta = \frac{1}{D^2}, \quad (5)$$

The stress (σ) is created by changing the lattice constant in the film. The stress (σ) was calculated from the X-ray diffraction data and the following formula [28]:

$$\sigma = \frac{E(a - a_0)}{2\nu a_0}, \quad (6)$$

where $E=200$ Gpa and $\nu=0.31$ are Young's modulus and the Poisson's ratio of the NiO, respectively. NiO column nanostructures are porous films and tensile stress is created due to cavities and porosities embedded in the nanostructure [29]. Compressive stress is caused by the growth of atomic close-packed columns in the structure of each column which is dominant in this work. The lattice parameter, grain size, strain, and stress of the NiO films are listed in Table 1.

TABLE 1.
STRUCTURAL PARAMETERS OBTAINED FOR NiO COLUMNAR NANOSTRUCTURE FROM XRD ANALYSIS

2θ(°)	(h k l)	FWHM (°)	d ($\mathring{A}$)	d_0 ($\mathring{A}$)	a ($\mathring{A}$)	a_0 ($\mathring{A}$)	ε(%)	D (nm)	δ	σ (Gpa)
37.44	(1 1 1)	0.52	2.35	2.40	4.07	4.15	-1.92	16.8	0.0035	-6.44
43.47	(2 0 0)	1.00	2.10	2.08	4.21	4.16	1.20	8.7	0.0132	4.26
63.20	(2 2 0)	0.30	1.43	1.47	4.06	4.15	-2.16	33.6	0.0008	-7.29
79.87	(2 2 2)	0.34	1.22	1.20	4.23	4.16	1.68	32.0	0.0009	6.28

a_0 and a is the bulk material and the measured lattice constant. ε, D, δ, and σ are strain, grain size, dislocation density, and stress, respectively.

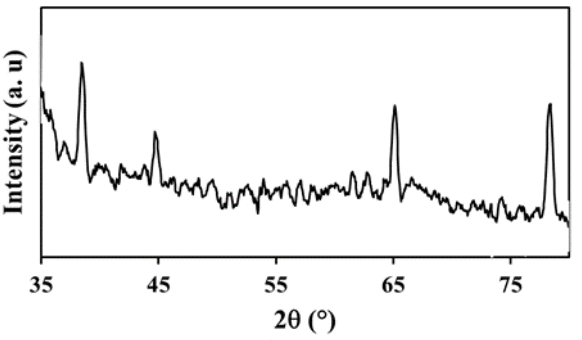

Fig. 1. XRD pattern of the NiO columnar nanostructure on the glass substrate

2) Field emission scanning electron microscope

The NiO columnar nanostructure morphology deposited on the glass substrate by the OAD technique was characterized from FESEM images. The top view FESEM photographs of NiO columnar nanostructure are shown in Fig. 2a. The bombardment of the sample by high-energy particles causes the crystals to merge and form coarse grains. The average grain size was about 64.85 nm, in good agreement with the XRD measurements of NiO columnar nanostructure. Fig. 2b shows the cross-sectional view FESEM image of the NiO columnar

nanostructure at a thickness of 490 ± 20 nm while the columns were tilted at a 35º angle. The average diameter of nanocolumn is obtained between 10-30 nm. The nickel oxide films deposited in a specific direction consist of atomic close-packed columns in the structure of each column with a porous surface that grows obliquely over the film surface. Due to the impact of high-energy NiO particles on the surface, the self-shadowing effect, and competitive growth, a continuous film is formed on the surface [30, 31].

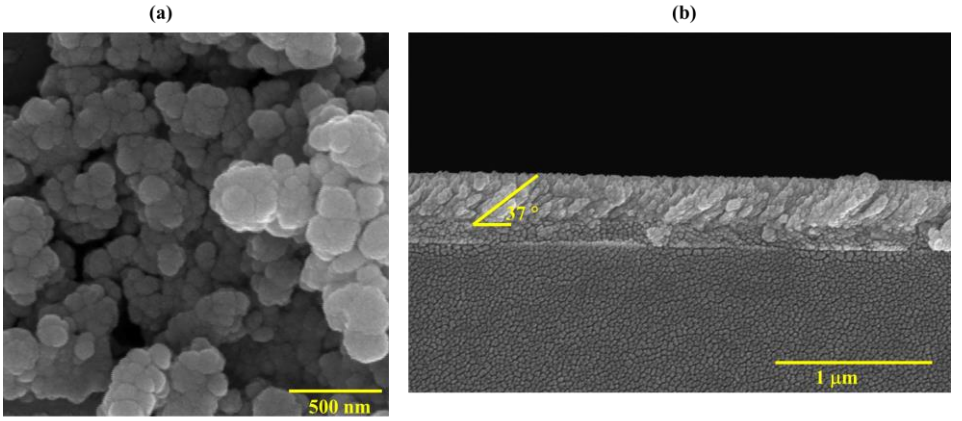

Fig. 2. FESEM pattern for the NiO columnar nanostructure, (a) top view at 500 nm (b) cross-sectional view of the film at 1µm.

B. Optical properties

1) Energy bandgap

Fig. 3 presents the spectral transmittance of the NiO columnar nanostructure on a glass substrate in the wavelength region of 200-1100 nm for deposition angle of 35 º. Horprathum et al. [23] showed that for deposition angles greater than 40 º, the transmittance decreases due to increased porosity and surface roughness. In fact, as the deposition angle increases, the film density decreases and the distance between the columns increases. The NiO columnar nanostructure has good transmittance about 85% in the wavelength region between 370 to 1100 nm due to a deposition angle of less than 40º as shown in Fig. 3a. On the other hand, large grains obtained in the FESEM image (about 64.85 nm) mean fewer grain boundaries and thus less scattering at the grain boundary. This would lead to a highly transparent nickel oxide film.

The graph of reflectance as a function of wavelength for the NiO columnar

nanostructure is shown in Fig. 3b. The reflection with the wavelength changes inversely with the transmittance. Reflection at 300 nm is sharply reduced from 94% to 15%.

The absorption coefficient of the film (α_f) can be obtained by using the film thickness (d_f), the transmittance of the bare substrate (T_s), transmittance (T), and reflectance (R) as follows [33]:

$$\alpha_f = \frac{1}{d_f}\ln\left(\frac{1-R}{T/T_s}\right). \quad (7)$$

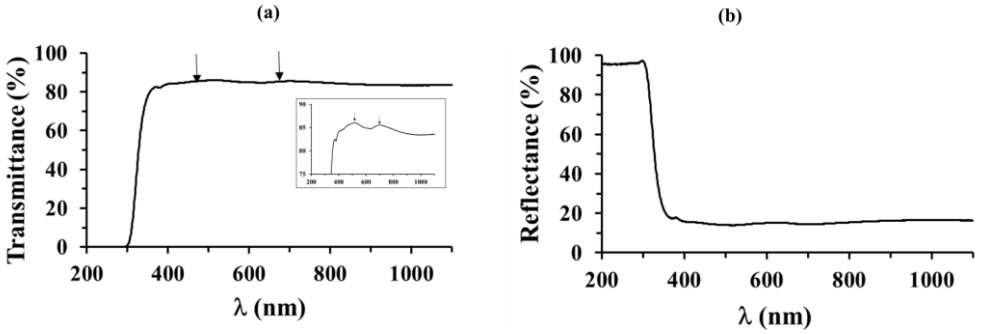

Fig. 3. (a) Optical transmittance spectra and (b) optical reflectance spectra as a function of wavelength of NiO columnar nanostructure.

Fig. 4a shows the absorption coefficient α as a function of wavelength in the spectral range of 350-1100 nm for the NiO columnar nanostructure on glass.

The optical bandgap (E_g) can be calculated for direct transmission by using Tauc's formula [33]:

$$\alpha h\nu = A(h\nu - E_g)^n, \quad (8)$$

where A is a constant and $h\nu$ is photon energy. At high photon energies, the transmittance changes linearly, so by extrapolating this linear section, the energy band gap can be determined. The value of the optical bandgap of the NiO columnar nanostructure was obtained at about 4.06 eV. The bandgap of nickel oxide films reported by researchers varies depending on the deposition conditions, the type of deposition, and its parameters. Kunz and Adler reported the energy bandgap for NiO films about 3.6 - 4 eV [34, 35]. In another study, NiO layers were fabricated by pyrolysis spray technique, and the energy band gap was measured from 3.75 to 3.97 eV [36]. Nandy [37] and Reddy [38] also reported the optical band gap of NiO films was about 3.82 at a power of 150 W with the sputtering method. According to the results, the residual strain can

change the band gap of a semiconductor. Tensile strain reduces the bandgap and the compressive strain increases it [39]. The average tensile strain in NiO columnar nanostructure is 1.4% while the average compressive strain is 2.04% according to XRD results (Table 1). Therefore, due to the compressive strain being greater than the tensile strain, the bandgap of this nanostructure is increased. Therefore, the increase in the bandgap obtained in this work compared to the thin film in previous research may be due to a change in the morphology of the structure.

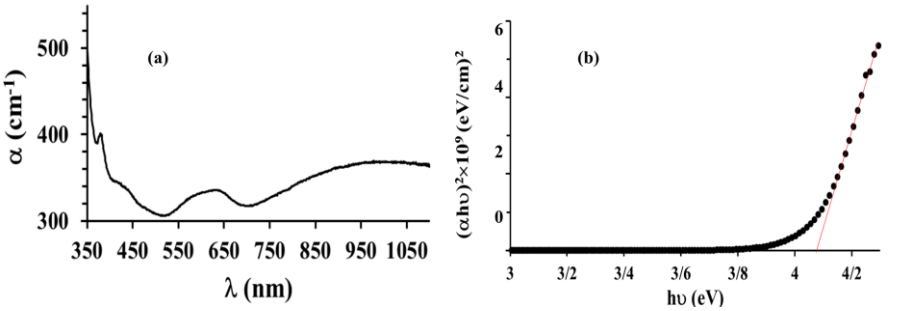

Fig. 4. (a) Absorption coefficient as a function of wavelength and (b) $(\alpha hv)^2$ as a function of hv of NiO columnar nanostructure.

2) Optical constants

The wavelength of the incident light and scattering can affect the optical constants, including the refractive index of the material. When an electromagnetic wave propagates in a medium, in addition to scattering the wave, it loses its energy and becomes damp.

Therefore, the refractive index is a complex function in terms of the frequency of the light. The complex refractive index ($n^*=n+ik$) consists of the real part n and the imaginary part k, which are called the dispersion and the extinction coefficient (including absorption and dispersion), respectively. They can be obtained using the following formula [40]:

$$k = \frac{\alpha\lambda}{4\pi}, \tag{9}$$

$$n = \left(\frac{1+R}{1-R}\right) - \left(\frac{4R}{(1-R)^2} - k^2\right)^{\frac{1}{2}}, \tag{10}$$

where R and λ are the reflectance of the film and the wavelength of the incident light, respectively.

The refractive index n and extinction coefficient k of NiO columnar nanostructure on glass is shown in Fig. 5. Fig. 5a shows that the extinction coefficient decreases sharply near the edge of the band in the visible region and then its value is almost constant. The extinction coefficient value at wavelengths greater than 300 nm is in the range of 0.001 to 0.004. The refractive index diagram (Fig. 5b) shows two absorption bands around the wavelengths of 520 and 700 nm, which indicates absorption at the absorption edges (Fig. 3a) shows the absorption edges with an arrow). The refractive indices at 520 and 700 nm are 2.19 and 2.22, respectively. Then, the refractive index increases from 2.22 at 700 nm to 2.35 at 920 nm and is approximately constant over 920 nm. Due to the high absorption value at low wavelengths, the refractive index is high. It is observed that the maximum refractive index at very low wavelengths (λ = 350 nm) is about n = 3. Usha [41] and Sawaby [42] reported the absorption edge around the wavelength of 500 nm for the NiO thin film having the lowest refractive index. The refractive index value in this study is higher at around 500 nm (absorption edge) due to the greater film thickness and structural morphology. The absorption edge is around 700 nm due to the morphology of the structure. Also, Sawaby [42] achieved a refractive index of 2.36 at a wavelength of about 850 nm, which is consistent with the results of this study.

It is worth noting that the refractive index depends on the film density and porosity. The porosity was calculated from the following relation [43]:

$$porosity(\%) = \left[1 - \left(\frac{n^2 - 1}{n_d^2 - 1}\right)\right] \times 100\%, \tag{11}$$

where n_d is the refractive index of NiO columnar nanostructure and n is the refractive index of NiO with cubic structure (2.18). The porosity is zero with n_d=n when we are dealing with a non-porous dense material. In completely porous materials, n_d tends to 1 and the porosity reaches its maximum value (porosity=1). At wavelengths greater than 350 nm, where the absorption rate is very low, the average porosity is obtained about 31%. Porosity depends on the shadowing effect and the angle of the columns with the substrate [44]. Therefore, the refractive index is related to the effect of defects and structural disorders. The porosity created in the nanostructure is due to tilted nanocolumns. However, each column has a structure of close-packed that increases the film density in the direction of growth. Therefore, increasing the density has increased the refractive index of this nanostructure compared to the work of Usha [41] and Sawaby [42].

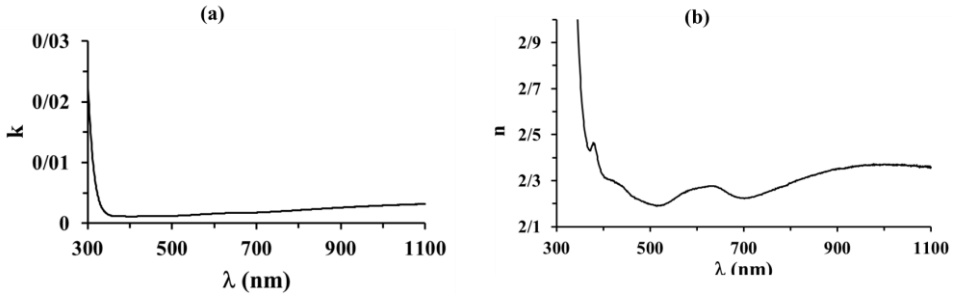

Fig. 5. (a) Extinction coefficient and (b) refractive index as a function of wavelength of NiO columnar nanostructure.

2) Dielectric constants

Electrons in the thin film are excited by light, which causes the complex dielectric constant to change with frequency. The real and real dielectric constants are associated with dispersion and dissipation, respectively.

The real and imaginary dielectric constants depend on *n* and *k*, which are defined as follows:

$$\varepsilon_r = n^2 - k^2, \tag{12}$$

$$\varepsilon_i = 2nk. \tag{13}$$

Fig. 6 shows ε_r and ε_i as a function of wavelength for the NiO columnar nanostructure. The real dielectric value at 520 and 700 nm are 4.80 and 4.94, respectively. Then, it increases from 4.94 at 700 nm to 5.54 at 920 nm and is approximately constant over 920 nm. The average value of ε_r in the visible region is about 0.0065 for the NiO columnar nanostructure on glass. Then its value increased slowly with increasing wavelength due to increasing the wave dissipation.

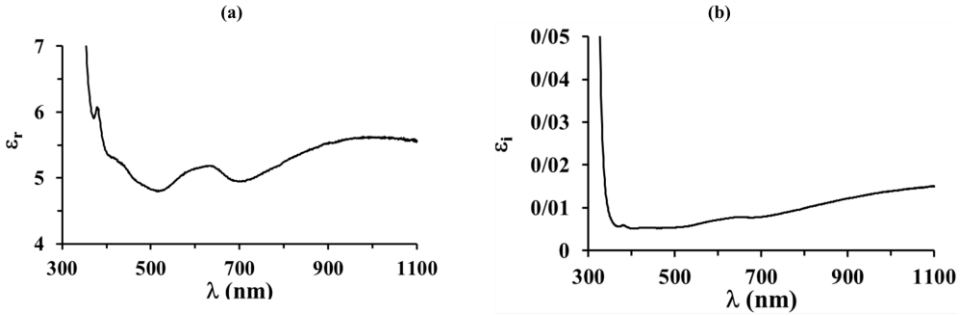

Fig. 6. (a) ε_r and (b) ε_i as a function of wavelength of NiO columnar nanostructure.

4. CONCLUSION

Optical characterization of the NiO columnar nanostructure on glass substrate has been investigated. The XRD diffraction peaks of the NiO columnar nanostructure showed that the prepared nanostructure has a face-centered lattice and polycrystalline nature. The transmittance spectrum of the NiO columnar nanostructure shows about 85% in the wavelength region between 370 to 1100 nm. The value of the optical bandgap of the nanostructure obtained was about 4.06 eV. The refractive index shows two absorption bands around the wavelengths of 520 and 700 nm with values of 2.19 and 2.22, respectively. Then, the refractive index increases from 2.22 at 700 nm to 2.35 at 920 nm and remains almost constant over 920 nm. The real dielectric value at 520 nm and 700 nm are 4.80 and 4.94, respectively. Then, it increases from 4.94 at 700 nm to 5.54 at 920 nm and is approximately constant over 920 nm. The results show that by controlling the deposition parameters and preparing the nanostructure with a pre-designed morphology, transparent conducting oxide (TCOs) can be prepared.

5. CONFILICT OF INTEREST

The authors declare that there is no conflict of interest regarding the publication of this manuscript.

REFERENCES

[1] H. Sato, T. Minami, S. Takata, T. Yamada. *Transparent conducting p-type NiO thin films prepared by magnetron sputtering*. Thin solid films. 236(1-2) (1993, Dec) 27-31. Available: http://doi.org/10.1016/0040-6090(93)90636-4.

[2] S. Ahmmed, A. Aktar, J. Hossain, A. B. Ismail. *Enhancing the open circuit voltage of the SnS based heterojunction solar cell using NiO HTL*. Solar Energy. 207 (2020, Sep) 693-702. Available: https://doi.org/10.1016/j.solener.2020.07.003.

[3] N. P. Klochko, V. R. Kopach, I. I. Tyukhov, D. O. Zhadan, K. S. Klepikova, G. S. Khrypunov, S. I. Petrushenko, V. M. Lyubov, M. V. Kirichenko, S. V. Dukarov, A. L. Khrypunova. *Metal oxide heterojunction (NiO/ZnO) prepared by low temperature solution growth for UV-photodetector and semi-transparent solar cell*. Solar Energy. 164 (2018, Apr) 149-59. Available: https://doi.org/10.1016/j.solener.2018.01.054.

[4] H. Azimi, S. H. Ahmadi, M. R. Manafi, S. H. Hashemi Moosavi, M. Najafi. *Development a simple and sensitive method for determination low trace of nickel by local surface plasmon resonance of citrate capped silver nanoparticles*. Journal of Optoelectronical Nanostructures. 6 (2021, May) 23-40. Available: https://doi.org/ 20.1001.1.24237361.2021.6.2.1.5.

[5] B. Kisan, J. Kumar, S. Padmanapan, P. Alagarsamy. *Defect induced ferromagnetism in NiO nanocrystals: Insight from experimental and DFT+ U study*. Physica B: Condensed Matter. 593 (2020, Sep) 412319. Available: https://doi.org/10.1016/j.physb.2020.412319.

[6] R. Balakarthikeyan, A. Santhanam, R. Anandhi, S. Vinoth, A. M. Al-Baradi, Z. A. Alrowaili, M. S. Al-Buriahi, K. D. Kumar. *Fabrication of nanostructured NiO and NiO: Cu thin films for high-performance ultraviolet photodetector*. Optical Materials. 120 (2021, Oct) 111387. Available: https://doi.org/10.1016/j.optmat.2021.111387.

[7] G. T. Phan, D. Van Pham, R. A. Patil, C. H. Tsai, C. C. Lai, W. C. Yeh, Y. Liou, Y. R. Ma. *Fast-switching electrochromic smart windows based on NiO-nanorods counter electrode*. Solar Energy Materials and Solar Cells. 231 (2021, Oct) 111306. Available: https://doi.org/10.1016/j.solmat.2021.111306.

[8] C. W. Lin, W. C. Chung, Z. D. Zhang, M. C. Hsu. *P-channel transparent thin-film transistor using physical-vapor-deposited NiO layer*. Japanese Journal of Applied Physics. 57(1S) (2017, Nov) 01AE01. Available: https://doi.org/ 10.7567/JJAP.57.01AE01.

[9] J. D. Hwang, T. H. Ho. Effects of oxygen content on the structural, *optical, and electrical properties of NiO films fabricated by radio-frequency magnetron sputtering*. Materials Science in Semiconductor Processing. 71 (2017, Nov) 396-400. Available: https://doi.org/10.1016/j.mssp.2017.09.002.

[10] T. Razegh, V. Setoodeh, S. Pilban Jahromi. *Influence of particle size on Magnetic behavior of nickel oxide nanoparticles*. Journal of Optoelectronical Nanostructures. 2 (2017, May) 11-18. Available: https://doi.org/ 20.1001.1.24237361.2017.2.2.2.8.

[11] S. Rafiee Rafat, Z. Ahangari, M. M. Ahadian, *Performance Investigation of a Perovskite Solar Cell with TiO2 and One Dimensional ZnO Nanorods as Electron Transport Layers*. Journal of Optoelectronical Nanostructures, 6 (2021, May) 75-90. Available: http://doi.org/ 20.1001.1.24237361.2021.6.2.6.0.

[12] P. Misra, V. K. Sahu, R. S. Ajimsha, A. K. Das, B. Singh. *Studies on resistive switching times in NiO thin films grown by pulsed laser deposition*. Journal of Physics D: Applied Physics. 50 (2017, Sep) 415106. Available: https://doi.org/10.1088/1361-6463/aa83ce.

[13] S. Chaoudhary, A. Dewasi, S. Ghosh, R. J. Choudhary, D. M. Phase, T. Ganguli, V. Rastogi, R. N. ereira, A. Sinopoli, B. Aïssa, A. Mitra. *X-ray photoelectron spectroscopy and spectroscopic ellipsometry analysis of the p-NiO/n-Si heterostructure system grown by pulsed laser deposition*. Thin Solid Films. 743 (2022, Feb) 139077. Available: https://doi.org/10.1016/j.tsf.2021.139077

[14] D. R. Sahu, Y. H. Lee, T. J. Wu, S. C. Wang, J. L. Huang. *Synthesis and electrochromic property improvement of NiO films for device applications*. Thin Solid Films. 707 (2020, Aug) 138097. Available: https://doi.org/10.1016/j.tsf.2020.138097.

[15] D. R. Sahu, T. J. Wu, S. C. Wang, J. L. Huang. *Electrochromic behavior of NiO film prepared by e-beam evaporation.* Journal of Science: Advanced Materials and Devices. 2 (2017, Jun) 225-32. Available: https://doi.org/10.1016/j.jsamd.2017.05.001.

[16] S. Manouchehri, J. Zahmatkesh, M. H. Yousefi. *Substrate effects on the structural properties of thin films of lead sulfide*. Journal of Optoelectronical Nanostructures. 32 (2018, June) 1-18. Available: https://doi.org/20.1001.1.24237361.2018.3.2.1.4

[17] M. Fakharpour, M. Gholizadeh Arashti, M. T. Musazade Meybodi. *Electrical characterization of zig-zag Aluminum thin films using experimental and theoretical methods*. Journal of Optoelectronical Nanostructures. 6 (2021, Aug) 25-42. Available: https://doi.org/10.30495/JOPN.2021.27468.1218.

[18] M. Fakharpour, H. Savaloni. *Fabrication of graded helical square tower-like Mn sculptured thin films and investigation of their electrical properties: comparison with perturbation theory*. Journal of Theoretical and Applied Physics. 2 (2017, Jun) 109-17. Available: https://doi.org/10.1007/s40094-017-0242-3.

[19] S. Sarkar, S. K. Pradhan. *Silica-based antireflection coating by glancing angle deposition*. Surface Engineering. 35 (2019, Nov) 982-5. Available: https://doi.org/10.1080/02670844.2019.1596578.

[20] V. Potin, H. Boukhalfa, N. Martin. *Oblique angle co-deposition of nanocolumnar tungsten thin films with two W sources: Effect of pressure and target current*. Materials Chemistry and Physics. 281 (2022, Apr) 125864. Available: https://doi.org/10.1016/j.matchemphys.2022.125864 .

[21] M. Tyagi, M. Tomar, V. Gupta. *Glad assisted synthesis of NiO nanorods for realization of enzymatic reagentless urea biosensor*. Biosensors and Bioelectronics. 52 (2014, Feb) 196-201. Available: https://doi.org/10.1016/j.bios.2013.08.020.

[22] V. Kannan, A.L. Inamdar, S. M. Pawar, H. S. Kim, H. C. Park, H. Kim, H. Im, Y. S. Chae. *Facile route to NiO nanostructured electrode grown by oblique angle deposition technique for supercapacitors*. ACS applied materials & interfaces. 8 (2016, Jul) 17220-5. Available: https://doi.org/10.1021/acsami.6b03714.

[23] M. Horprathum, C. Chananonnawathorn, J. Kaewkhao, N. Sangwaranatee. *Nanostructure NiO films grown by oblique angle deposition*. Suranaree Journal of Science & Technology. 27 (2020, Jan).

[24] H. L. Chen, Y. M. Lu, W. S. Hwang. *Thickness dependence of electrical and optical properties of sputtered nickel oxide films*. Thin Solid Films. 498 (2006, Mar) 266-70. Available: https://doi.org/10.1016/j.tsf.2005.07.124.

[25] M. V. Kumar, S. Muthulakshmi, A. A. Paulfrit, J. Pandiarajan, N. Jeyakumaran, N. Prithivikumaran. *Structural and optical behaviour of thermally evaporated p-type nickel oxide thin film for solar cell applications*. Int. J. Chem. Tech. Res. 6 (2014) 5174-7.

[26] M. Awais, M. Rahman, J. D. MacElroy, N. Coburn, D. Dini, J. G. Vos, D.P. *Dowling. Deposition and characterization of NiOx coatings by magnetron sputtering for application in dye-sensitized solar cells*. Surface and Coatings Technology. 204 (2010, May) 2729-36. Available: https://doi.org/10.1016/j.surfcoat.2010.02.027.

[27] T. Obata, K. Komeda, T. Nakao, H. Ueba, C. Tatsuyama. *Structural characterization of Si0. 7Ge0. 3 layers grown on Si (001) substrates by molecular beam epitaxy*. Journal of applied physics. 81 (1997, Jan) 199-204. Available: https://doi.org/10.1063/1.363841.

[28] M. Ohring. *The Material Science of Thin Solid Films*. New York: Academic Press, 2001.

[29] W. Buckel. *Internal stresses*. Journal of Vacuum Science and Technology. 6(4) (1969, Jul) 606-9. Available: https://doi.org/10.1116/1.1315702.

[30] M. Horprathum, T. Srichaiyaperk, B. Samransuksamer, A. Wisitsoraat, P. Eiamchai, S. Limwichean, C. Chananonnawathorn, K. Aiempanakit, N. Nuntawong, V. Patthanasettakul, C. Oros. *Ultrasensitive hydrogen sensor based on Pt-decorated WO3 nanorods prepared by glancing-angle dc magnetron sputtering*. ACS Applied Materials & Interfaces. 24(6) (2014, Dec) 22051-60. Available: https://doi.org/10.1021/am505127g.

[31] C. Oros, M. Horprathum, A. Wisitsoraat, T. Srichaiyaperk, B. Samransuksamer, S. Limwichean, P. Eiamchai, D. Phokharatkul, N. Nuntawong, C. Chananonnawathorn, V. Patthanasettakul. *Ultra-sensitive NO2 sensor based on vertically aligned SnO2 nanorods deposited by DC reactive magnetron sputtering with glancing angle deposition technique*. Sensors and Actuators B: Chemical. 223 (2016, Feb) 936-45. Available: https://doi.org/10.1016/j.snb.2015.09.104.

[32] M. Cesaria, A. P. Caricato, M. Martino. *Realistic absorption coefficient of ultrathin films*. Journal of Optics. 14(10) (2012, Aug) 105701. Available:https://doi.org/ 10.1088/2040-8978/14/10/105701.

[33] J. Tauc, R. Grigorovici, A. Vancu. *Optical properties and electronic structure of amorphous germanium*. physica status solidi (b). 15(2) (1966) 627-37. Available: https://doi.org/10.1002/pssb.19660150224.

[34] A. B. Kunz. *Electronic structure of NiO*. Journal of Physics C: Solid State Physics. 14(16) (1981, Jun) L455. Available: https://doi.org/10.1088/0022-3719/14/16/001.

[35] D. Adler, J. Feinleib. *Electrical and optical properties of narrow-band materials*. Physical Review B. 2(8) (1970, Oct) 3112. Available: https://doi.org/10.1103/PhysRevB.2.3112.

[36] S. A. Mahmoud, A. A. Akl, H. Kamal, K. Abdel-Hady. *Opto-structural, electrical and electrochromic properties of crystalline nickel oxide thin films prepared by spray pyrolysis*. Physica B: Condensed Matter. 311(3-4) (2002, Feb) 366-75. Available: https://doi.org/10.1016/S0921-4526(01)01024-9.

[37] S. Nandy, U. N. Maiti, C. K. Ghosh, K. K. Chattopadhyay. *Enhanced p-type conductivity and band gap narrowing in heavily Al doped NiO thin films deposited by RF magnetron sputtering*. Journal of Physics: Condensed Matter. 21(11) (2009, Feb) 115804. Available: https://doi.org/10.1088/0953-8984/21/11/115804.

[38] A. M. Reddy, A. S. Reddy, K. S. Lee, P. S. Reddy. *Growth and characterization of NiO thin films prepared by dc reactive magnetron*

sputtering. Solid State Sciences. 13(2) (2011, Feb) 314-20. Available: https://doi.org/10.1016/j.solidstatesciences.2010.11.019.

[39] R. Deng, B. Yao, Y. F. Li, Y. Xu, J. C. Li, B. H. Li, Z. Z. Zhang, L. G. Zhang, H. F. Zhao, D. Z. Shen. *Ultraviolet electroluminescence from n-ZnO/p-NiO heterojunction light-emitting diode*. Journal of luminescence. 134 (2013, Feb) 240-3. Available: https://doi.org/10.1016/j.jlumin.2012.08.039.

[40] A. A. Al-Ghamdi, W. E. Mahmoud, S. J. Yaghmour, F. M. Al-Marzouki. *Structure and optical properties of nanocrystalline NiO thin film synthesized by sol–gel spin-coating method*. Journal of Alloys and compounds. 486(1-2) (2009, Nov) 9-13. Available: https://doi.org/10.1016/j.jallcom.2009.06.139.

[41] K. S. Usha, R. Sivakumar, C. Sanjeeviraja. *Optical constants and dispersion energy parameters of NiO thin films prepared by radio frequency magnetron sputtering technique*. Journal of Applied Physics. 114(12) (2013 Sep) 123501. Available: https://doi.org/10.1063/1.4821966.

[42] A. Sawaby, M. S. Selim, S. Y. Marzouk, M. A. Mostafa, A. Hosny. *Structure, optical and electrochromic properties of NiO thin films*. Physica B: Condensed Matter. 405(16) (2010, Aug) 3412-20. Available: https://doi.org/10.1016/j.physb.2010.05.015.

[43] B. E. Yoldas. *Investigations of porous oxides as an antireflective coating for glass surfaces.* Applied Optics. 19(9) (1980, May) 1425-9. Available: https://doi.org/ 10.1364/ AO.19.001425.

[44] L. G. Daza, M. Acosta, R. Castro-Rodriguez, A. Iribarren. *Tuning optical properties of ITO films grown by rf sputtering: effects of oblique angle deposition and thermal annealing.* Transactions of Nonferrous Metals Society of China. 29(12) (2019, Dec) 2566-76. Available: https://doi.org/10.1016/S1003-6326(19)65164-2.